Evaluation of Microstructure and Hardness of Novel Al-Fe-Ni Alloys with High Thermal Stability for Laser Additive Manufacturing

I.S. Loginova, Marjolaine Sazerat, P.A. Loginov, A.V. Pozdniakov, N.A. Popov, A.N. Solonin

Evaluation of Microstructure and Hardness of Novel Al-Fe-Ni Alloys with High Thermal Stability for Laser Additive Manufacturing

I.S. LOGINOVA ,[1,2,4] M.V. SAZERAT,[2,3] P.A. LOGINOV,[2] A.V. POZDNIAKOV,[2] N.A. POPOV,[1] and A.N. SOLONIN[2]

1.—Ural Federal University, 19, Mira Street, Ekaterinburg, Russian Federation 620002. 2.—National University of Science and Technology "MISiS", 4, Leninsky Ave, Moscow, Russian Federation 119991. 3.—IMT Mines Albi, Allée des sciences, Albi 81000, France. 4.—e-mail: loginova@misis.ru

The microstructure and phase composition of cast and laser-melted Al-Fe-Ni alloys were investigated. Two main phases—$Al_3(Ni,Fe)$ and Al_9FeNi—were formed in the as-cast state. A fine microstructure without porosity or solidification cracks was observed in the Al-Fe-Ni alloys after laser treatment. The hardness of the laser-melted alloys was 2.5–3 times higher than the hardness of the as-cast alloys owing to the formation of an aluminum-based solid solution and fine eutectic particles. The formation of the primary Al_9FeNi phase was suppressed as a result of the high cooling rate. Annealing these alloys at temperatures less than 300°C demonstrated the high thermal stability of the microstructure while maintaining the hardness. The Al-Fe-Ni alloys investigated in this study are promising heat-resistant materials for additive manufacturing because of their fine, stable structure, and the low interdiffusion coefficients of Fe and Ni.

INTRODUCTION

Additive manufacturing (AM) technologies offer the capability to produce parts with improved properties. Selective laser melting (SLM) and direct metal deposition (DMD) are the most common technologies used to manufacture parts from metal powders. In both technologies, parts are formed layer by layer from the powder upon laser beam impact.[1–3] Aluminum (Al) alloys, having low density and desirable mechanical and technological properties, are good candidates for AM.

The list of Al alloys suitable for AM is increasing every year and currently includes powders in the following forms: Al-Si (AlSi12,[4] AlSi10Mg,[5] AlSi7Mg[6]), Al-Mg-Sc (Al-6.2Mg-0.36Sc-0.09Zr,[7] Al-4.6Mg-0.66Sc-0.42Zr-0.49Mn [8]), Al-Zn-Mg (AA7075,[9] AA7050[10]), and Al-Cu-Mg (Al-3.5Cu-1.5Mg-1Si[11]). However, only AlSi10Mg alloy and Al-4.6Mg-0.66Sc-0.42Zr-0.49Mn alloy (Scalmalloy) powders are currently being used in commercial applications. The latter material is conducive to the laser melting process because of its narrow effective solidification range and the presence of a sufficiently large amount of aluminum–silicon eutectic in the structure, as well as the high content of zirconium and scandium. The AlSi10Mg alloy has substantially lower strength than the Scalmalloy but is significantly less expensive. The Al-Cu and Al-Cu-Mg alloys exhibit relatively high strength at both room and elevated temperatures.[12] However, the drawback of using these alloys in AM lies in their poor casting properties and weldability.[13–16]

Aluminum alloys with transition metals are prospective heat-resistant material options for applications at 300–350°C.[2,17–20] The development of novel material compositions with strong mechanical and technological properties, especially at elevated temperatures, is currently a focus point for AM. Alloying with transition metals such as Mn, Cr, Fe, Ni, and Ce has been shown to increase high-temperature strength and improve the casting properties of Al alloys.[2,16,18,19] A negative outcome when alloying with transition metals is the formation of coarse primary intermetallic particles. However, the ultra-high cooling rate of 10^3–10^5 K/s

helps to inhibit the nucleation and recrystallisation of primary intermetallic particles.[21–23] Another advantage of the high cooling rate is the potential formation of a supersaturated solid solution (SSSS). Stability of the SSSS is one of the most important factors for heat-resistant alloys. The stability of both the SSSS and intermetallic phases depends on the rate of diffusion of the alloying elements in the Al solid solution. Good candidates for Al alloying are Fe and Ni because of their low diffusion coefficients (7×10^{-13} and 2×10^{-12}[24] in Al at 500°C, respectively), which are less than one-third of the diffusion coefficients of the main alloying elements (Mg, Cu, Zn, Si).

Alloying of Al with Fe and Ni has attracted great interest in this system in applications of AM, in particular for selective laser melting. Slow-cooled Al-Fe-Ni alloys are characterized by coarse primary brittle intermetallic phases.[25] Such structural features may impair the mechanical properties of these materials, confining their application. Hence, a high cooling rate, that can be realized in AM, can solve this problem. Alloying with nickel and iron improves the high-temperature mechanical properties[26] of the Al_3Fe, Al_3Ni and Al_9FeNi intermetallic phases.[27] A high Ni content is beneficial in cases of selective laser melting because the formation of Al_9FeNi primary crystals can be suppressed.

The development of new alloys for AM technologies is associated with the complexity of the manufacture of the powders, the optimization of the production technology, and the high cost of the equipment. However, the development of powders is a classical material science task, in which it is important to understand the structure formation processes after laser treatment. The impact is characterized by the following features: high local temperature leading to the melt of a small volume of metal, and subsequent fast cooling under conditions of directional heat removal.[7] These features determine the basic principles of the formation of the structure and properties of products produced by selective laser melting and direct laser deposition.[20] These features can be simulated on a simple laser machine using bulk samples[18] that allow the analysis of the basic principles of structure formation of the alloys without the application of powder materials.

In the present work,the laser melting of Al-Fe-Ni bulk metal was used as a method of simulation of SLM and DLD melting and solidification conditions to analyze the formation of the microstructure of laser-melted Al-Fe-Ni alloys during solidification and heat treatment.

MATERIALS AND METHODS

Novel Al-2.5Fe-5.5Ni, Al-2.5Fe-7.5Ni, and Al-2.5Fe-9.5Ni alloys were prepared by melting a mixture of pure Al (99.99%), Al-10Fe master alloy, and Al-20Ni master alloy in a Nabertherm S3 electric furnace at 780°C. In order to check the chemical composition of the alloys, we carried out energy-dispersive x-ray spectroscopy (EDS) analysis of the large areas of polished samples: 1 × 1 mm. The real composition was practically identical: Al-2,4%Fe-5,7%Ni, Al-2,5%Fe-7.6%Ni, and Al-2,9%Fe-9,3%Ni. These concentrations of alloying components were chosen after the analysis of the ternary phase diagram of the Al-Fe-Ni system: all the alloys were located in the phase region: (Al), Al_3(Fe,Ni), and Al_9FeNi. As the Ni content increases, the fraction of the heat-resistant Ni-containing phase Al_3(Fe,Ni) should also increase, leading to increases in the strength and heat resistance of the alloys. Although the Al_9FeNi phase forms as coarse crystals under equilibrium conditions, in fast crystallization during laser melting, the Al_9FeNi formation can be suppressed leading to the formation of SSSS with high mechanical properties.

Ingots with the size of 40 × 20 × 120 mm^3 were cast into a water-cooled copper mold. The cooling rate of the as-cast ingot was approximately 10 K/s. The cooled ingots were cut into 2-mm-thick plates for laser melting.

The liquidus and solidus temperatures were determined by differential scanning calorimetry (DSC) on a Setaram Labsys calorimeter in an argon atmosphere. The time dependence of the temperature difference between the cell with the sample and the reference cell was measured experimentally using an S-type (platinum:platinum–rhodium) thermocouple. The measurement error was ± 1°C. The experiments were carried out in the 20–800°C temperature range at a constant heating rate (1°C/s).

Laser melting of single tracks was carried out on the 2-mm-thick plates using an MUL-1-M-200 machine equipped with an Nd-YAG fiber laser (1064 nm wavelength) under the following parameters: laser power 150 W, scan speed 1 mm/s, overlap distance 0.2 mm, and an argon atmosphere. These parameters provided an average volumetric energy density of approximately 50 J/mm^3. The alloys were heat-treated in a Nabertherm N30/65A electric furnace.

The volume of the eutectic phases in the as-cast state was determined by using Axis Visual software. The size of the dendritic cells was measured using the linear intercept method according to the Russian standard 21073.0-75.

To determine the phase composition and to calculate the lattice parameter in the specimens that were laser-melted and annealed at 500°C for 1 h, x-ray powder diffraction (XRD) analysis was performed using a Brucker Advance D8 x-ray diffractometer. For the XRD studies, we prepared special square specimens of 1 mm thickness. The specimens were laser-melted through their whole surface and thickness. The XRD results of the laser-melted and laser-melted/annealed specimens were provided to confirm that the Al_9FeNi phase was suppressed.

Annealing at 500°C for 1 h was chosen to complete the solid solution decomposition, which was observed by means of transmission electron microscopy (TEM; JEOL 2100) and energy-dispersive x-ray spectroscopy (EDX; XMAX-80). The microstructure, chemical composition, and phase composition of the alloys were analyzed by scanning electron microscopy (SEM; TESCAN VEGA 3LMH) in conjunction with EDS. The structures of the foils were investigated by TEM at 200 kV. Specimens with a diameter of 3 mm were prepared using the A2 electrolyte on Struers Tenupol-5 equipment.

To analyze the heat resistance of the investigated alloys in laser-melted condition the next regimes were used: annealing at 100°C, 200°C, 250°C, 300°C, 350°C, 400°C, and 500°C for 1 h, at 250°C for 1, 2, 3, 4, 8, 16, and 20 h, and at 300°C for 1, 2, 3, 4, 8, 16, and 20 h.

Vickers hardness (HV) measurements were performed on a Wolpert 402MVD hardness tester.

RESULTS AND DISCUSSION

The microstructures of the alloys in the as-cast state are presented in Fig. 1. The dendrites of the Al-based solid solution and of the primary crystals of Al_9FeNi phase are the main microstructural elements in the as-cast state. The two phases that form the secondary eutectic were identified as $Al_3(Ni,Fe)$ and Al_9FeNi ($30 \times 400\ \mu m^2$ grains in Fig. 1d). As the Ni concentration increased from 5.5% to 9.5%, the volume percentage of the eutectic increased from 24% to 37% (Fig. 1a–c).

For the alloys used in AM, the solidification range is extremely important.[28–30] Solidification cracking is closely related to the range of the solidification temperature and the content of liquid phases. In the current work, the comparison between the solidification intervals of Al-Fe-Ni and AlSi10Mg (the most popular alloy in SLM[20]) alloys were carried out (Table I). Liquidus and solidus temperatures and the solidification range of the Al-Fe-Ni alloys were detected by DSC and are presented in Table I.

The investigated alloys have a narrow solidification range that can provide good casting properties and weldability. Also, the Al-Fe-Ni alloys have much higher solidus temperatures than AlSi10Mg (Table I) which provide high heat resistance.

A typical SEM image of the microstructure of the laser-melted single tracks tested is shown in Fig. 2. A structure without porosity and solidification cracks was formed in the Al-Fe-Ni alloys being investigated. The formation of the primary Al_9FeNi phase was suppressed owing to the high cooling rate. Figure 3 provides TEM images of the microstructure of the laser-melted single tracks. An Al-based solid solution and fine eutectic origin particles were present in the microstructure. EDX analyses of the TEM images confirms the formation of $Al_3(Ni,Fe)$ (Fig. 3d). The mean sizes of the dendritic cells of the primary Al were 165 nm, 80 nm, and 27 nm in the Al-2.5Fe-5.5Ni, Al-2.5Fe-7.5Ni, and Al-2.5Fe-9.5Ni alloys, respectively. A decrease of the dendritic cell average size in the alloys may be attributed to a change in the crystallization conditions. It has been shown that, as the Ni concentration increases, the solidification range decreases (Table I). Under the same cooling conditions, provided by one laser melting mode, the degree of supercooling will be higher in the Al-2.5Fe-9.5Ni alloy compared to the Al-2.5Fe-5.5Ni alloy, leading to the appearance of more crystallization nuclei and the refinement of the microstructure. A quasi-eutectic structure was found in the Al-2.5Fe-9.5Ni alloy (Fig. 3c), which features a similar mean size of the dendritic cells and eutectic phase particles (10–70 nm). The lattice parameters of the Al-based solid solutions in the laser-melted and annealed specimens measured via XRD are shown in Table II. The lattice parameter of the Al solid solution decreases with the Ni content from 0.40487 nm in the Al-2.5Fe-5.5Ni alloy to 0.40465 nm in the Al-2.5Fe-9.5Ni alloy. The reduction of the lattice parameter in Al is associated with the dissolution of Ni in it by the substitution method. This was presumably due to the increase in the Ni content in the Al solid solution given that the atomic radius of Ni[24] is 0.019 nm smaller than that of Al.[24] After annealing, the lattice parameters approached that of pure Al (99.99%), which is 0.40491 nm.[24] This indicates the decomposition of a supersaturated Al-based solid solution followed by the formation of a secondary Ni-containing phase. The XRD analysis of the samples after annealing showed that the intensity of the peaks of the $Al_3(Fe,Ni)$ phase increases (see Supplementary Fig. S1) indicating an increase in the concentration of this phase in the alloys. Hence, the secondary phase has the same structure as the eutectic.

The hardness in the as-cast state for the Al-2.5Fe-5.5Ni, Al-2.5Fe-7.5Ni and Al-2.5Fe-9.5Ni alloys are 53, 58, and 65 HV, respectively. A slight tendency for the hardness to possibly increase can be associated with an increase of the primary crystal size and the volume of the eutectic phases. The structural refinement and formation of a SSSS leads to a significant increase in hardness, by more than a factor of 3, compared to the as-cast alloys (see Supplementary Fig. S2).

Annealing of the alloys at lower temperatures (below 300°C) demonstrated the high thermal stability of the microstructure and the hardness (Figs. 4, 5). HV curves of the Al-Fe-Ni alloys after annealing at 100°C, 200°C, 250°C, 300°C, 400°C, and 500°C for 1 h, 250°C for 1–20 h, and 300°C for 1–20 h are presented in Fig. 4. The hardness slightly decreased after a -h annealing at temperatures below 300°C, but fell drastically at higher

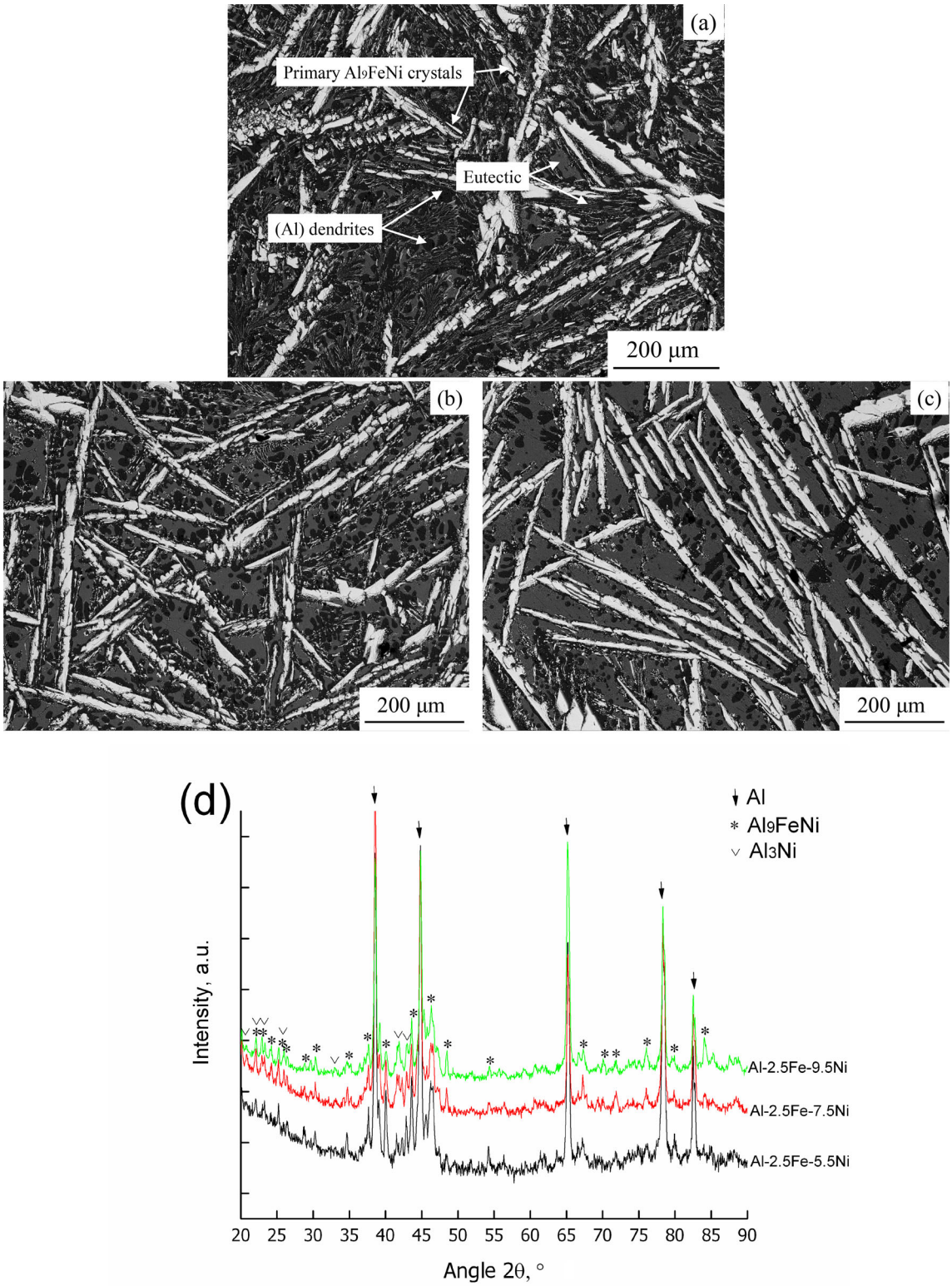

Fig. 1. SEM image of (a) Al-2.5Fe-5.5Ni, (b) Al-2.5Fe-7.5Ni, and (c) Al-2.5Fe-9.5Ni alloys, and (d) XRD patterns of the Al-Fe-Ni alloys in the as-cast state.

Table I. Liquidus and solidus temperatures and the solidification range of the Al-Fe-Ni alloys (experimental data)

Alloy	Liquidus temperature, °C	Solidus temperature, °C	Solidification range, °C
Al-2.5Fe-5.5Ni	641	635	6
Al-2.5Fe-7.5Ni	641	638	3
Al-2.5Fe-9.5Ni	641	639	2
AlSi10Mg 31	578	557	21

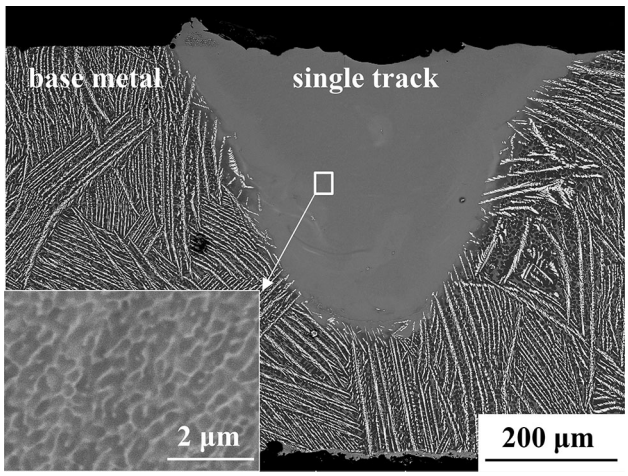

Fig. 2. SEM image of a single track of Al-Fe-Ni alloys.

Table II. Lattice parameters of Al solid solutions of laser-melted and laser-melted/annealed areas

Alloy	Condition	Å	ΔÅ
Al-2.5Fe-5.5Ni	Laser-melted	4.0487	0.0008
	Laser-melted/annealed	4.0496	
Al-2.5Fe-7.5Ni	Laser-melted	4.0480	0.0015
	Laser-melted/annealed	4.0495	
Al-2.5Fe-9.5Ni	Laser-melted	4.0465	0.0030
	Laser-melted/annealed	4.0495	

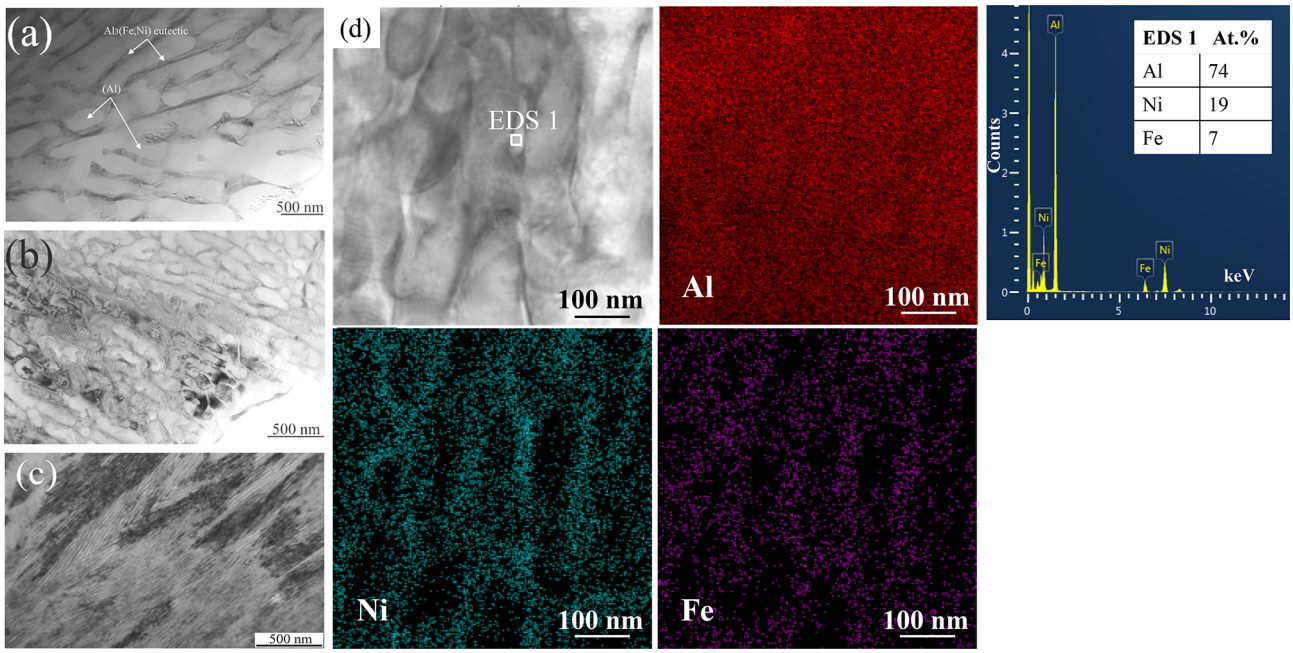

Fig. 3. TEM images of single tracks in (a) Al-2.5Fe-5.5Ni, (b) Al-2.5Fe-7.5Ni, and (c) Al-2.5Fe-9.5Ni alloys, and (d) Fe and Ni distribution maps of the Al-2.5Fe-7.5Ni alloy.

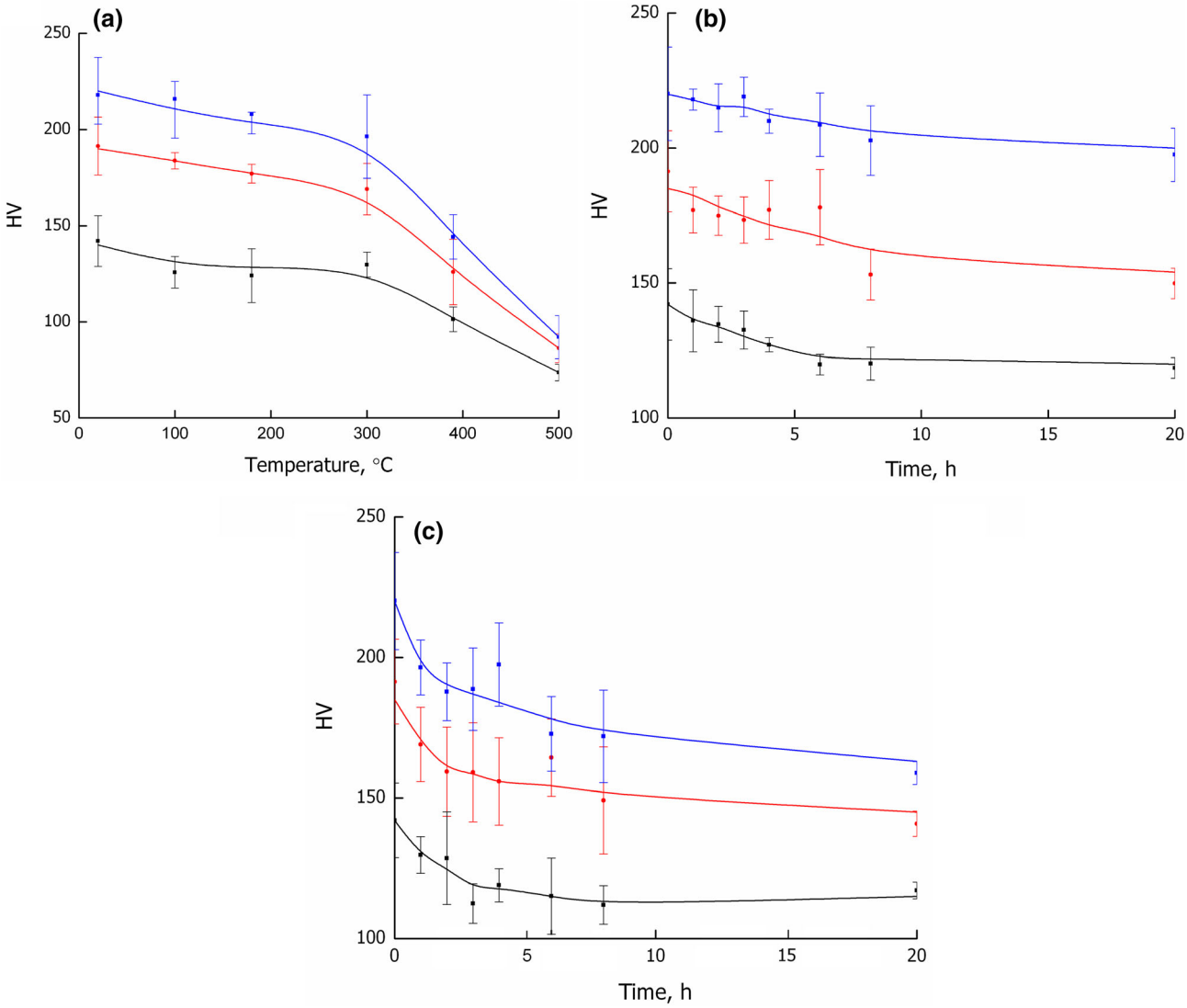

Fig. 4. HV curves of Al-Fe-Ni alloys after annealing at (a) 100–500°C for 1 h, (b) 250°C for 120 h, and (c) 300°C for 1–20 h. The black line is Al-2.5Fe-5.5Ni, the red line is Al-2.5Fe-7.5Ni, and the blue line is Al-2.5Fe-9.5Ni.

annealing temperatures (Fig. 4a). Annealing at 250°C and 300°C resulted in a slight decrease in HV after 1–5 h and stabilisation of HV up to 20 h. Softening at low temperatures (e.g., 300°C) could be due to the decrease in the as-cast dislocation density and partial decomposition of the SSSS. The size and morphology of the intermetallic phases after annealing at 250°C for 20 h and 300°C for 1 h experienced no significant changes (Fig. 5a, b). The sharp decrease in hardness after a 1-h annealing at 500°C can be explained by the fragmentation and growth of the intermetallic phases (Fig. 5c), and the full decomposition of the supersaturated Al solid solution (Table II). The size of the eutectic phase particles increased to 100–300 nm after annealing at 500°C for 1 h (Fig. 5c),and the lattice parameter increased up to the value of pure Al (Tables II, III).

CONCLUSIONS

The microstructure and phase composition of as-cast and laser-melted Al-Fe-Ni alloys were investigated by SEM, TEM, and XRD. $Al_3(Ni,Fe)$ and Al_9FeNi phases formed in the as-cast alloys. A structure without porosity or solidification cracks was formed in the Al-Fe-Ni alloys after laser treatment. The hardness of the laser-melted alloys was 2.5–3 times higher than the hardness of the as-cast alloys. An Al-based solid solution and fine eutectic particles were present in the microstructure. The formation of the primary Al_9FeNi phase was suppressed due to the high cooling rate. The mean size of the dendritic cells of the primary Al in the Al-2.5Fe-5.5Ni, Al-2.5Fe-7.5Ni, and Al-2.5Fe-9.5Ni alloys were 165 nm, 80 nm and 27 nm, respectively. The size of the eutectic particles

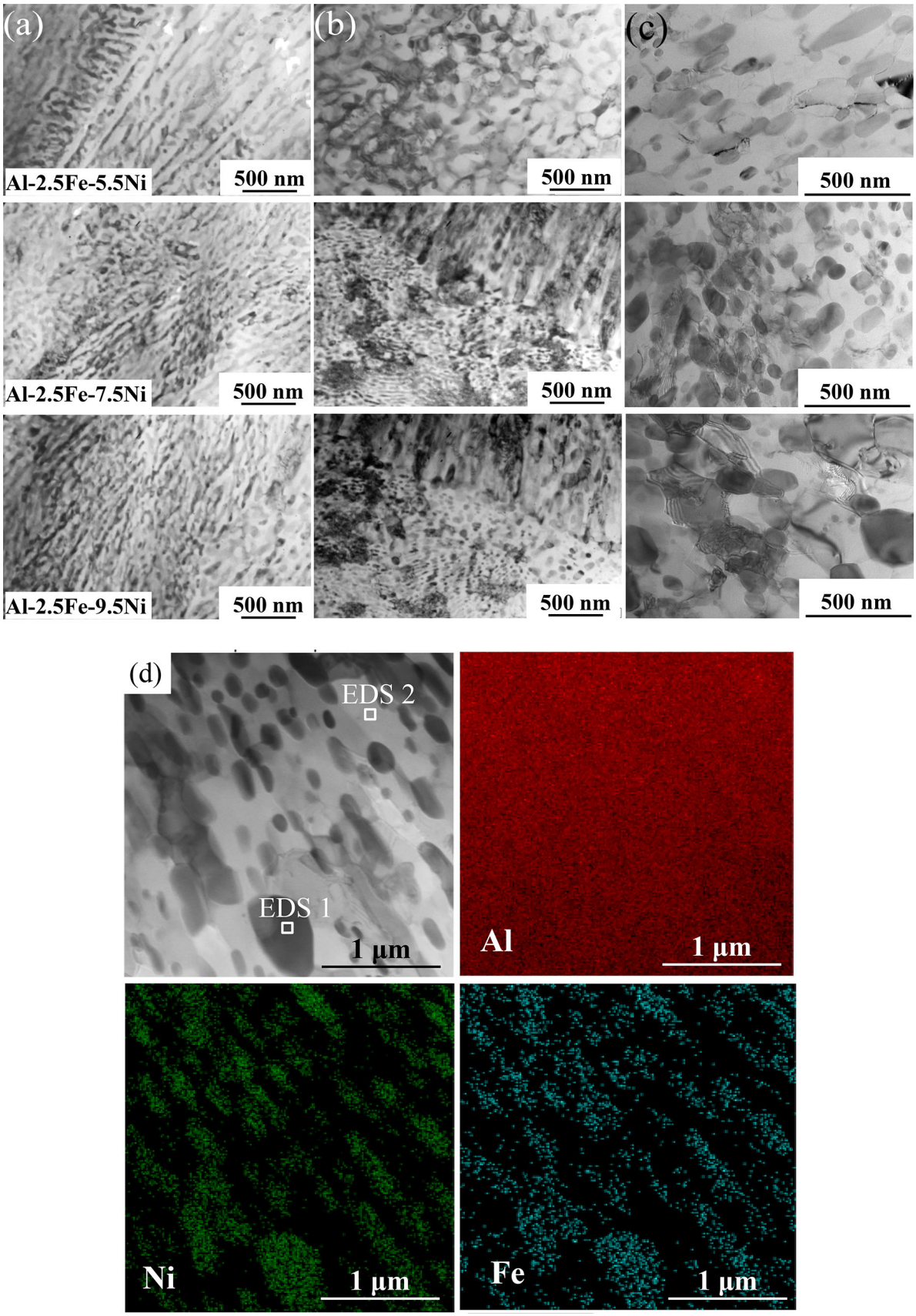

Fig. 5. TEM images of single tracks of Al-Fe-Ni alloys after annealing at (a) 250°C for 20 h, (b) 300°C for 1 h, and (c) 500°C for 1 h, and (d) Fe and Ni distribution maps of the Al-2.5Fe-7.5Ni alloy after annealing at 500°C 1 h.

Table III. EDS results of the Al-2.5Fe-7.5Ni alloy after annealing at 500°C for 1 h

	Chemical composition, at.%		
	Al	Ni	Fe
EDS 1	71	23	6
EDS 2	100	0	0

ranged from 10 nm to 70 nm. The Ni content in the Al solid solution increased with the Ni content in the alloy because the atomic radius of the Al is smaller than that of Ni. Annealing of the investigated alloys at lower temperatures (below 300°C) demonstrated the high thermal stability of the microstructure and the hardness. Annealing at 250°C and 300°C leads to a slight decrease in HV after 1–5 h and stabilization of the HV up to 20 h. The softening could be due to the decrease in the as-cast dislocation density and the partial decomposition of a SSSS. The size and morphology of the intermetallic phases after annealing at 250°C for 20 h and 300°C for 1 h changed insignificantly. The Al-Fe-Ni alloys investigated in this study are promising high-strength and heat-resistant materials for AM because of their fine, stable structure and low diffusion rates of Fe and Ni.

ACKNOWLEDGEMENTS

Loginova I.S. would like to thank Dr. Solonin A.N. for valuable discussions regarding the structure formation process. This project and all the experiments were funded by RFBR, Project Number 19-38-60037.

CONFLICT OF INTEREST

The authors declare that they have no conflict of interest.

ELECTRONIC SUPPLEMENTARY MATERIAL

The online version of this article (https://doi.org/10.1007/s11837-020-04321-2) contains supplementary material, which is available to authorized users.

REFERENCES

1. A.V. Pozdniakov, AYu Churyumov, I.S. Loginova, D.K. Daubarayte, D.K. Ryabov, and V.A. Korolev, *Mater. Lett.* 225, 33 (2018). https://doi.org/10.1016/j.matlet.2018.04.077.
2. D.R. Manca, AYu Churyumov, A.V. Pozdniakov, D.K. Ryabov, V.A. Korolev, and D.K. Daubarayte, *Mater. Lett.* 236, 676 (2019). https://doi.org/10.1016/j.matlet.2018.11.033.
3. AYu Churyumov, A.V. Pozdniakov, A.S. Prosviryakov, I.S. Loginova, D.K. Daubarayte, D.K. Ryabov, V.A. Korolev, A.N. Solonin, M.D. Pavlov, and S.V. Valchuk, *Mater. Res. Express* 6, 126595 (2019). https://doi.org/10.1088/2053-1591/ab5bea.
4. R.A. Rahman, A. Haider, S. Palanisamy, and S.H. Masood, *Mater. Today Proc.* 4, 8724 (2017). https://doi.org/10.1016/j.matpr.2017.07.221.
5. C.A. Biffi, J. Fiocchi, P. Bassani, D.S. Paolino, A. Tridello, G. Chiandussi, M. Rossetto, and A. Tuissi, *Procedia Struct. Integrity* 27, 50 (2017). https://doi.org/10.1016/j.prostr.2017.11.060.
6. M. Wang, B. Song, Q. Wei, Y. Zhang, and Y. Shi, *Mater. Sci. Eng. A* 739, 463 (2019). https://doi.org/10.1016/j.msea.2018.10.047.
7. R. Li, M. Wang, T. Yuan, B. Song, C. Chen, K. Zhou, and P. Cao, *Powder Technol.* 319, 117 (2017). https://doi.org/10.1016/j.powtec.2017.06.050.
8. A.B. Spierings, K. Dawson, T. Heeling, P.J. Uggowitzer, R. Schäublin, F. Palm, and K. Wegener, *Mater. Des.* 115, 52 (2017). https://doi.org/10.1016/j.matdes.2016.11.040.
9. B. Jiang, L. Zhenglong, C. Xi, L. Peng, L. Nannan, and C. Yanbin, *Ceram. Int.* 45, 5680 (2019). https://doi.org/10.1016/j.ceramint.2018.12.033.
10. T. Qi, H. Zhu, H. Zhang, J. Yin, L. Ke, and X. Zeng, *Mater. Des.* 135, 257 (2017). https://doi.org/10.1016/j.matdes.2017.09.014.
11. P. Wang, C. Gammer, F. Brenne, K. Gokuldoss Prashanth, R. Gregorio Mendes, M. Hermann Rümmeli, T. Gemming, J. Eckert, and S. Scudino, *Mater. Sci. Eng. A* 711, 562 (2018). https://doi.org/10.1016/j.msea.2017.11.063.
12. ASM HANDBOOK, *Properties and Selection: Nonferrous Alloys and Special-Purpose Materials*, vol. 2 (The Materials Information Company, 2010).
13. O. Lopez-Botello, U. Martinez-Hernandez, J. Ramírez, C. Pinna, and K. Mumtaz, *Mater. Des.* 113, 369 (2017). https://doi.org/10.1016/j.matdes.2016.10.031.
14. V.S. Zolotorevskiy, A.V. Pozdniakov, and Y.Y. Kanakidi, *Russ. J. Non. Ferrous Met.* 53, 392 (2012). https://doi.org/10.3103/S1067821212050148.
15. V.S. Zolotorevskiy, A.V. Pozdniakov, and A.V. Khvan, *Russ. J. Non. Ferrous Met.* 52, 50 (2011). https://doi.org/10.3103/S1067821211010275.
16. A.V. Pozdniakov and V.S. Zolotorevskiy, *Int. J. Cast Met. Res.* 27, 193 (2014). https://doi.org/10.1179/1743133613Y.0000000096.
17. N. Kaufmann, M. Imran, T.M. Wischeropp, C. Emmelmann, S. Siddique, and F. Walther, *Phys. Procedia* 83, 918 (2016). https://doi.org/10.1016/j.phpro.2016.08.096.
18. A. Plotkowski, O. Rios, N. Sridharan, Z. Sims, K. Unocic, R.T. Ott, R.R. Dehoff, and S.S. Babu, *Acta Mater.* 126, 507 (2017). https://doi.org/10.1016/j.actamat.2016.12.065.
19. Q. Jia, P. Rometsch, P. Kürnsteiner, Q. Chao, A. Huang, M. Weyland, L. Bourgeois, and X. Wu, *Acta Mater.* 171, 108 (2019). https://doi.org/10.1016/j.actamat.2019.04.014.
20. J. Zhang, B. Song, Q. Wei, D. Bourell, and Y. Shi, *J. Mater. Sci. Technol.* 35, 270 (2019). https://doi.org/10.1016/j.jmst.2018.09.004.
21. Q. Jia, P. Rometsch, S. Cao, K. Zhang, and X. Wu, *Mater. Des.* 174, 107775 (2019). https://doi.org/10.1016/j.matdes.2019.107775.
22. M. Rappaz, B. Carrupt, M. Zimmermann, and W. Kurz, *Helv. Phys. Acta* 60, 924 (1987). https://doi.org/10.5169/seals-115877.
23. W. Kurz and R. Trivedi, *Metall. Mater. Trans. A* 27A, 625 (1996). https://doi.org/10.1007/BF02648951.
24. K. Hirano, R. Aagrwala, and M. Cohen, *Acta Metall.* 10, 857 (1962). https://doi.org/10.1016/0001-6160(63)90172.
25. B.L. Silva, J.G. Dessi, L.F. Gomes, M.M. Peres, M.V. Cante, and J.E. Spinelli, *J. Alloys Compd.* 691, 952 (2017). https://doi.org/10.1016/j.jallcom.2016.08.243.
26. S. Engin, U. Büyük, and N. Maraslı, *J. Alloys Compd.* 660, 23 (2016). https://doi.org/10.1016/j.jallcom.2015.11.080.

27. N.A. Belov, D.G. Eskin, and N.N. Avxentieva, *Acta Metall.* 53, 4709 (2005). https://doi.org/10.1016/j.actamat.2005.07.003.
28. X. Cao, W. Wallace, J.P. Immarigeon, and C. Poon, *Mater. Manuf. Process.* 18, 1 (2003). https://doi.org/10.1081/amp-120017586.
29. J.M. Sánchez-Amaya, T. Delgado, L. González-Rovira, and F.J. Botana, *Appl. Surf. Sci.* 255, 9512 (2009). https://doi.org/10.1016/j.apsusc.2009.07.081.
30. H. Zhang, H. Zhu, X. Nie, J. Yin, Z. Hu, and X. Zeng, *Scr. Mater.* 134, 6 (2017). https://doi.org/10.1016/j.scriptamat.2017.02.036.
31. M. Vončina, P. Mrvar, and J. Medved, *Mater. Geoenviron. J.* 52, 621 (2006).